Multi-scale design of novel materials for emerging challenges in active thermal management: open-pore magnesium-diamond composite foams with nano-engineered interfaces

J.M. Molina-Jordá

PII: S1359-835X(17)30427-X
DOI: https://doi.org/10.1016/j.compositesa.2017.11.020
Reference: JCOMA 4841

To appear in: *Composites: Part A*

Received Date: 25 April 2017
Revised Date: 30 October 2017
Accepted Date: 23 November 2017

Please cite this article as: Molina-Jordá, J.M., Multi-scale design of novel materials for emerging challenges in active thermal management: open-pore magnesium-diamond composite foams with nano-engineered interfaces, *Composites: Part A* (2017), doi: https://doi.org/10.1016/j.compositesa.2017.11.020

Multi-scale design of novel materials for emerging challenges in active thermal management: open-pore magnesium-diamond composite foams with nano-engineered interfaces

J.M. Molina-Jordá

Instituto Universitario de Materiales de Alicante and Departamento de Química Inorgánica, Universidad de Alicante, Ap. 99, E-E03080, Spain

E-mail address: (jmmj@ua.es)

ABSTRACT

Open-pore Mg foams, which have been traditionally discarded for heat dissipation applications given their low thermal conductivity values, can prove appealing materials for active thermal management if they incorporate diamond particles coated with a nano-dimensioned layer of TiC. These composite foam materials can be manufactured by the replication method, conveniently adapted to Mg, that requires a strict multi-scale control: correct distribution of structural constituents (pores, diamond and Mg) on the meso-/micro-scale ensures homogeneity and complete pore connectivity, while a proper nanoscale control of the TiC coating on diamond particles achieves high thermal conductance at the interface between diamond particles and Mg. The manufactured Mg-diamond foam materials attain outstanding thermal conductivity values (up to 82 W/mK) and maximum heat dissipation performance, tested on active convective cooling, almost two times higher than their equivalent magnesium foams and twenty per cent superior to that of conventional aluminium foams.

Keywords: Metal-matrix composites (MMCs); Foams; Thermal properties; Liquid metal infiltration

1. Introduction

Thermal management has become a critical issue that often slows down, or even hinders, the progress of emerging technologies in power electronics [1-3]. Increasing power densities and diminishing transistor dimensions are hallmarks of modern electronics that demand an accelerating research progress in novel materials that allow heat dissipation [1]. Passive (or phase change material) thermal management is being extensively explored by developing novel composite materials with high thermal conductivity. Among this class of materials, those based on metal matrices and diamond particles with nano-engineered interfaces are noteworthy for their excellent thermal conductivity values (see [4-6] for aluminium-matrix and [7] for Mg-matrix composite materials). Despite the main disadvantage of active (air- or liquid-cooling) thermal management sometimes needing equipment overdesign, it has proven to be advantageous to enhance heat transfer efficiency in electronic devices. For those applications, the use of foam materials in which air or cooling liquids are forced to pass through their porous structure to remove heat by convection has been extensively evaluated [8-15] (research includes aluminium [9-11] and copper foams [12,13], among those of a metallic nature, and carbon/graphite foams [14,15], which have lately attracted much attention given their low density). These materials, which generally outperform similar dense material configurations [8], must combine high solid-phase thermal conductivity to entrain heat deep into the solid structure of foam and a suitable heat transfer coefficient with the coolant in order to sweep away heat by passing fluid. The heat transfer behaviour of several tested foams (with porosities generally over 85%) is strongly related with pore geometry characteristics [11,16] and performs better as the number of pores lowers [10], as does the thermal conductivity [16]. For the forthcoming generation of materials for active thermal management, it seems consequently necessary

to work in two directions: i) on the one hand, we must consider denser foam materials capable of combining a high heat transfer coefficient, while maintaining sound thermal conductivity ([11] was demonstrated the good performance in the active cooling of aluminum foams with porosities within the 66-69% range); ii) on the other hand, the foamability of monolithic materials needs to move on to new complex materials based on developments of multiphase and multiscale designs with improved thermal properties.

Mg and its alloys have always been overlooked or discarded for thermal management because their thermal conductivity values are much lower than aluminium, silver or copper metals. However, a recent publication has shown that the combination of pure Mg and diamond particles coated with TiC generates composites of high thermal conductivity [7] capable of attracting candidates for passive thermal management (TiC coatings on diamond particles have also proven to enhance the metal–diamond interface thermal conductance for metals such as Al [17] and Cu [18,19]). Another issue that can be a disadvantage of Mg-based materials is their relatively easy degradation under corrosive environments. Nevertheless the authors of [20], in the aim of fabricating Mg foams for bioimpants, demonstrated that a coating of magnesium oxide successfully enhances the corrosion performance of these materials.

In this paper, we produced and characterised new foam materials whose skeleton consisted of a Mg-diamond composite with a nano-dimensioned TiC interface. To manufacture these materials the replication method, traditionally used for metal foaming, was followed. A porous preform made by the compaction of a mixture of large NaCl particles that touch one another and TiC-coated small diamond particles, located at the voids of NaCl particles, was infiltrated with pure Mg. Subsequently, NaCl particles were removed by dissolution in an aqueous solution of NaOH at pH 13. The

resultant materials attained high thermal conductivity values (up to 82 W/mK) and a heat dissipation capacity, which was tested on active convective cooling, that was almost two times higher than their equivalent Mg foams and twenty per cent superior to that of conventional aluminium foams.

2. Predictive schemes

A set of analytical models was used to predict the following items of interest: i) the volume fraction of bimodal mixtures of particles; ii) the heat thermal conductance of nanodimensoned interfaces; iii) the thermal conductivity of Mg-diamond composite foams. Details of each predictive scheme are provided below.

2.1 Volume fraction of the bimodal particle compacts

The volume fraction of the compacts conformed by particles of two different sizes of any average size ratio (bimodal mixtures) has been proved to well account for using the well-known Yu and Standish model [21]. This predictive scheme has proven to accurately fit different sets of experimental data [5,7,21,22] and is described by the following equation:

$$\left(\frac{v - v_c X_c}{v_s}\right)^2 + 2G\left(\frac{v - v_c X_c}{v_s}\right)\left(\frac{v - X_c - v_s X_s}{v_c - 1}\right) + \left(\frac{v - X_c - v_s X_s}{v_c - 1}\right)^2 = 1 \quad (1)$$

where v is the apparent volume occupied by the unit solid volume of particles (i.e., the reciprocal of the particle packing volume fraction V) and X is the fraction of an inclusion type in the bimodal particle mixture. Subscripts c and s refer to coarse and small particles, respectively, and G is a parameter that relates to the particle size ratio, which can be accounted for with the following empirical formula [23]:

$$G = 1 - (1 - v_l)^{0.63}\left(\frac{v_c}{v_s - v_c v_s}\right)^{-0.63} + \left(\frac{1}{R}\right)^{-1.89} \quad (2)$$

where *R* is the ratio coarse-to-small particle radius.

2.2 Thermal conductance of nanodimensioned interfaces

The thermal conductance (h) of Mg-TiC-diamond interfaces can be estimated by the following equation, derived from an electrical analogy model [7]:

$$\frac{1}{h_{Mg-TiC-D}} = \frac{1}{h_{Mg-TiC}} + \frac{TiC\ thickness}{K_{TiC}} + \frac{1}{h_{TiC-D}} \quad (3)$$

To use Equation (3), the data in Table 1 are necessary (the qualities of the Mg metal and diamond particles used in this work are the same as those used in the cited references). Table 1 also contains information on the Mg-diamond interface, which is necessary for predictive purposes on composites that contain uncoated diamond particles.

2.3 Thermal conductivity of magnesium-diamond composite foams

The thermal conductivity of Mg-diamond composite foam materials can be predicted with the Generalised Differential Effective Medium Scheme (GDEMS), which has been applied successfully to model and interpret thermal conduction in different composite materials [5,7,26,27]. The leading integral equation of the GDEMS approach for a multi-phase composite material is

$$\int_{K_m}^{K_c} \frac{dK}{K\sum_i X_i \frac{-\left(K - K_r^{eff}\right)}{\left(K - K_r^{eff}\right)P - K}} = -ln(1 - V) \quad (4)$$

where *K* is thermal conductivity and subscripts *c* and *m* refer to composite and matrix, respectively. X_i is the fraction of the *i* inclusion type in the total amount of inclusions of the composite (in these materials we consider two types of inclusions: diamond particles (D) and pores (P); hence $X_D+X_P=1$). *V* is the total volume fraction of inclusions and *P* is the polarisation factor of an inclusion (equal to 0.33 for spheres, as modelled in this study). K_r^{eff} is the effective thermal conductivity of an inclusion which, for spherical

geometries, is related to its intrinsic thermal conductivity, K_r^{in}, the matrix-inclusion interface thermal conductance *h*, and the radius of the inclusion *r*, by

$$K_r^{eff} = \frac{K_r^{in}}{1 + \frac{K_r^{in}}{hr}} \quad (5)$$

In general, the integral on the left-hand side of Eq. (1) has no analytical solution and needs to be solved numerically with appropriate mathematical software.

3. Experimental procedures

3.1 Materials

High purity magnesium (>99.9 wt%) was purchased from Goodfellow Metals, Cambridge, UK, with nominal major impurities shown in Table 2. Two sets of particles were used: diamond particles of MBD4 quality and two different average sizes of 36 μm and 24 μm, of a cubo-octahedral shape, purchased from Qiming (China), plus cubic NaCl particles of analytical quality (99.5% purity) acquired from Sigma-Aldrich (Riedstr, Switzerland). NaCl particles, originally of 300-400 μm, were ground and sieved to obtain fractions of narrower particle size distributions, from which those within the 350-400 μm range were selected. Table 3 provides the main characteristics of the powders. The SEM micrographs of the NaCl and MBD4 diamond particles are presented in Figure 1a-b.

Diamond particles were used for two conditions: i) as-received; and ii) TiC-coated. The coating was achieved by a heat treatment at 750°C of diamond particles in a salt melt with fine titanium powder (325 mesh that corresponds to an average size of about 45 μm, purchased from Alfa Aesar GmBH, Germany) in an argon atmosphere [7,28]. The salt mixture composition is given in Table 4 (all the chemicals were of analytical grade and purchased from AppliChem GmBH, Germany).

3.2 Manufacturing magnesium-diamond composite foams

The Mg-diamond composite foams were manufactured by following the replication method. This method involves the pressure infiltration of a liquid metal into the open space of a packed preform that can later be eliminated by dissolution. In the present case, the preforms were produced by packing mixtures of large NaCl particles and TiC-coated small diamond particles. The architecture of the preforms is such that NaCl particles touch one another and diamond particles are located in the voids left by NaCl particles (see Figure 1e-f for a schematic diagram of the replication method followed). Preparation of compacts turned out to be one of the most delicate aspects of the experimental procedures. Particle mixtures were packed into graphite crucibles of 17 mm inner diameter by repeatedly adding a small amount of powder, which was compacted by alternative strokes of a falling piston and vibrations (see [22] for details of the tap-packing procedure).

A solid Mg piece was placed inside the graphite crucible on top of the packed preform. To ensure successful infiltration, a special device was necessary, which has been recently patented for infiltrations with Mg and other liquid metals with intrinsic high vapour pressures [29,30]. This device, which is easy to adapt to any conventional infiltration apparatus, basically consists of a saturation crucible arranged to be inverted to the graphite crucible, it covers this crucible, which forms a closed saturation chamber. Magnesium metal was molten in a vacuum atmosphere (0.1 mbar) and infiltrations were performed at a temperature of 740ºC and a pressure of 2.5 MPa (applied with Ar gas). The total liquid metal-preform contact time was about 12 min, after which the sample was directionally solidified by moving the crucible with the sample to the bottom part of the infiltration chamber, which acted as a chiller. Samples were extracted from the graphite crucible and were placed for 10 min in a magnetically

stirred aqueous solution of NaOH (pH=13). With this, the NaCl particles located in the outermost regions of samples were diluted and samples became partially porous. Samples were then fitted into rubber tubes to allow the same basic solution pressurised at 4 bar to pass through the partially porous structure of samples in order to accelerate the dissolution of the internal NaCl particles. Complete NaCl dissolution was achieved in less than 3 min.

3.3 Chemical and microstructural characterisation

The composition of the TiC coating that covered the diamond particles was studied by X-ray diffraction (JSO-DEBYEFLEX 2002 Seifert diffractometer) and Auger Electron Spectroscopy (AES, VG-Microtech Multilab 3000). X-ray diffractograms were recorded using Cu Kα radiation at 40 kV and 40 mA within the 30-80º range (2θ) with a step of 0.05º and at a scan rate of 1º/min. The AES analyses were recorded as a function of sample depth with the help of a source of electrons and ions for automated charge balancing and an argon ion source for high-precision etching. The sputtering rate was maintained at 30 nm/min based on the calibration experiments performed by sputtering SiO_2 thin films.

Mg-diamond composite foams were observed under a Scanning Electron Microscope (SEM, Hitachi S-3000N) for microstructural characterisation. Samples were prepared by either fracturing materials under flexural effort or first fracturing and then removing the magnesium metal by electrochemical etching (current densities of 2.6 A/cm^2 and exposure times of 1.5 min were applied [7]). The interface and the surface of the diamond particles were chemically analysed by an Energy-dispersive X-ray Spectroscopy (EDX) analyser coupled to the SEM microscope.

3.4 Thermal characterisation of magnesium-diamond composite foams

The thermal conductivity of the materials was measured by a relative steady-state technique in an experimental set up that was assembled at the laboratories of the University of Alicante following the ASTM E-1225-04 International Standard (see [31] for a detailed explanation). The equipment basically consists of a clamping system able to establish a thermal gradient over a sample and a reference that are in contact across their cross sections. The reference material is in contact with a brass block that in its turn is connected to a thermally stabilized hot water bath at 70 ºC. The sample is connected to a water-cooled copper block at 20 ºC. Reference and sample are protected with thermal insulating materials in order to insure that heat losses through radiation and/or convection are minimized. A reference of brass alloy, with a thermal conductivity at 40ºC of 120 W/mK and cylindrical geometry (diameter of around 16 mm and length of 40 mm) was used. A non-silicon heat transfer paste (HTCP, Electrotube, Leicestershire, United Kingdom) was used to insure proper thermal contact when samples were clamped in between the brass reference and the copper block. The overall uncertainty of the measured thermal conductivities was estimated to be less than ±5%.

No standardised methodology exists to test heat sinks in induced-convection active thermal management. The design of the experimental setup used herein (Figure 2) was inspired by that proposed in [9]. In this device, an air flow is forced to pass through foam, which remains in contact with a hot surface so that air can take part of the heat transferred to foam by conduction and remove it by forced convection. The device is equipped with ten thermocouples located along height H (15 mm) of the sample. Five thermocouples come into contact with the sample and measure its temperature at each point. The other five thermocouples are located close to the sample, 2 mm apart from its

surface, and measure the temperature of the air that leaves the interior of the foam. There are two other thermocouples, T1 and T2, distanced at 35 mm, and located in the copper piece that leads the heat from the heating system to the sample. The heating system operates to control the temperature of the T2 thermocouple at 90ºC. The imposed air flow was regulated by a flow meter at 30 l/min of the maximum rate. The air flow regimes (in l/min) used in the present experiments were fixed at 3, 5, 7.5, 10, 15 and 20. When a specific air flow was set, the system needed about 15 minutes to reach a steady-state regime, after which different temperatures were noted. The thermal gradient in the copper reference piece can be related to the heat dissipation power density P (W/cm^2) of the sample by the following equation (equal heat flux through the reference and sample and negligible heat losses were assumed, provided that the reference was thermally isolated and that the reference and sample both had similar diameters):

$$P = k\frac{dT}{dx} \tag{6}$$

K is the thermal conductivity of the reference material (in the present case, K for 99.99% copper equalled 398 W/mK) and dT/dx is the thermal gradient in the copper reference.

4. Results and discussion

4.1 Selection of compositions of bimodal particle mixtures

Calculations of the packing volume fraction for the combinations of NaCl and diamond particles were made with the help of Equations 1-2 for the different R parameter values (ratio of the diameters of coarse NaCl particles to small diamond particles). The results of these calculations are depicted in Figure 3a for the entire spectrum of a fraction of NaCl particles in the bimodal mixtures. The shaded area shows the region of interest in

the present work. The particle systems that fell in this area were integrated by the large NaCl particles touching each other (which is essential to ensure their later dissolution) and smaller diamond particles accommodated in the voids left by the large NaCl particles. This area was delimitated by two experimental facts: i) a ratio between average particle sizes above seven is usually accepted to be the value above which small particles can accommodate in the free volume left by coarse particles [32]; ii) the volume fraction of large NaCl particles must be above 67% to guarantee that NaCl particles come into physical contact with each other [22,32].

In order to ensure that the experimental deviations from ideality in particle packing did not alter the continuity of the NaCl particulate architecture, two largely superior R values 10 and 15 were selected for the purpose of our experiments (see Table 3). Figure 3b displays a magnification of the region of interest (the shaded region in Figure 3a) along with the experimental results measured for the combinations of NaCl particles with either the MBD4 400-500 (R=10) or MBD4 600-700 (R=15) diamond particles. The results in Figure 3b are independent on the coating condition of the diamond particles since the TiC coating is thin enough not to significantly modify the geometry, and hence the packing efficiency, of the diamond particles. The agreement reached between the calculated and experimental results was sufficiently good to support the validity of Equations 1-2. The experimental results of Figure 3b were checked as being identical for either coated or uncoated diamond particles given the extremely narrow TiC coatings compared to the diamond particles diameters.

4.2 TiC coating on diamond particles

According to Equation 3, the interfacial thermal conductance of Mg-TiC-diamond interfaces ($h_{Mg\text{-}TiC\text{-}D}$) can be calculated from the h values for the Mg-TiC ($h_{Mg\text{-}TiC}$) and

TiC-diamond (h_{TiC-D}) interfaces, respectively, and the thickness and thermal conductivity of the TiC layer (calculations are plotted in Figure 4). Figure 4 provides the value of $h_{Mg-TiC-D}$ obtained in [7], which equalled 5.69×10^7 W/m^{2}K and corresponded to an interface with a TiC coating of low crystalline or chemical quality (with an ascribed low thermal conductivity of 18 W/mK) and a thickness of about 160 nm. Since the coating procedure used herein was the same as that followed in [7] (originally proposed in [28]), a similar thermal conductivity of about 18 W/mK was expected for the present TiC coatings. In this scenario, it became evident that a way to improve interface thermal conductance *h* found in [7] for the Mg-TiC-diamond system consisted in diminishing TiC thickness as much as possible (which is the equivalent to graphically moving left along the broken line of Figure 4). Based on different attempts, the present work found that homogeneous TiC coatings were obtained for a thickness of about 50 nanometers. According to this experimental fact, a proper treatment time of 25 min was selected to obtain TiC coatings with a thickness of about 50 nm. By considering a thermal conductivity of 18 W/mK for the TiC phase and using Equation (3) and the data in Table 1, the value for $h_{Mg-TiC-D}$ was calculated to equal 8.43×10^7 W/m^{2}K (which corresponded to log h = 7.92 in Figure 4).

Figure 5 shows a representative elemental profile analysis of the TiC-coated diamond particles performed by the AES technique. The sputtering depth shown as the x-axis was deduced from the sputtering time and rate. As seen in this figure, there are three main zones based on the element distribution of Ti and C along the depth. Zone A, which is the outer region of the surface to a depth of about 40 nm, presents an atomic Ti:C ratio of roughly 1:1, with a slight excess of titanium. This corresponds to a stoichiometry of approximately TiC (TiC is a highly non-stoichiometric compound which can crystallize in phases with slight defect of C (TiC_y with $0.5<y<0.98$) [33]. At

the outermost region of the zone A there is a much higher excess of titanium, probably caused by the presence of a mixture of TiC_y and unreacted Ti. The depth of second region, labelled as B, is about 10 nm and the atomic ration Ti:C varies from 1:1 near zone A to 1:0 at approximately a depth of 50 nm. This region corresponds to a transition layer from the outer TiC region to the diamond inner region. The inner zone, called C in Figure 5, corresponds to a composition of almost 100% C, which is indicative that the diamond substrate was achieved. A total of ten AES analysis were performed in different points and diamond particles and similar conclusions were obtained, giving an average thickness of the TiC coating of 50±7 nm.

From these data, two main conclusions were drawn: i) the composition of the coating on the diamond particles corresponded to TiC stoichiometry; ii) the thickness of this coating was about 50 nm. Composition Ti:C 1:1 can be further checked by the XRD technique (Figure 6). The pattern showed some residual unreacted Ti phase, which perfectly agreed with the observations from the AES analysis profile that the probable composition is TiCy, along with small unreacted Ti contents at the outermost region of TiC particles coating.

4.3 Magnesium-diamond composite foams

The Mg-matrix composite materials that contained NaCl and diamond particles for both the as-received and TiC-coated conditions were manufactured and characterised by measuring their density before and after NaCl particle dissolution. Figure 7 depicts the optical photographs and SEM micrographs of the Mg-diamond foams in which different items are worth mentioning.

A careful examination by scanning electron microscopy allowed us to appreciate that the porosity along the height of foams was homogeneous in all cases, which indicated

no clear signs of particle segregation in the preforms. Figure 7c depicts the details of the distribution of NaCl and diamond particles before NaCl dissolution. Diamond particles were located at positions which, after NaCl particles dissolution, corresponded with the struts of the foam materials (Figure 7d). Note that particles were homogeneously distributed in the Mg matrix and free of any visible damage (i.e. particle breaking) that could be caused by the strokes applied during the packing procedure. The magnesium metal did not show any indication of chemical corrosion, probably because the use of a basic solution for NaCl dissolution generated an oxygen-rich passivating coating on its surface, similar to those obtained by other passivation treatments [20].

As observed in [7] for the Mg-matrix composites with diamond particles of the same MBD4 quality, no clear sign of any reaction product was noted since the formation of the two possible binary magnesium carbides, MgC_2 and Mg_2C_3, was endothermic and most unlikely at the present processing temperatures (740ºC) [34]. There were, however, specific noteworthy details of the chemical composition of the diamond particle surfaces. Micrographs 7g and 7h, which are close looks at the diamond-Mg interface, reveal two distinct types of precipitates, which appear on diamond surfaces: one has a branched structure and corresponds to Si; the other one appears as small spots and corresponds to Fe. These fine precipitates were also present on the TiC coating that covered the diamond particles (Figure 7i and 7j). Silicon and iron were present as trace elements in the nominal composition of the magnesium metal, likely because their segregation at the interface occurred during post-infiltration metal solidification. Their presence at the diamond-Mg interface could strongly influence interfacial thermal conductance.

The micrographs of Figures 7e and 7f evidence that metal infiltration was complete since Mg filled the whole empty space of the porous particulate architecture. The

density measurements taken on samples prior to NaCl dissolution (values reported in Table 5) confirmed that metal saturation, defined as the amount of metal in the material divided by the amount of metal to fulfil the preform was, in all cases, within an error close to 100%. Table 5 also reports the density measurements for the foam materials (once NaCl was leached), which are in line with complete NaCl particle dissolution. Complete NaCl removal was also confirmed by the XRD measurements taken on some randomly selected samples since no NaCl peaks in their X-ray diffraction patterns were found.

4.4 Thermal conductivity of magnesium-diamond composite foams

Figure 8a shows the calculated thermal conductivity values for Mg-diamond composite foams in which the amount and size of diamond particles, along with the TiC coating thickness on diamond particles, varied. Calculations were made with Equations (1-9) and data are reported in Table 1. Some important features emerge from Figure 8. First it was noted that a larger fraction and average size of diamond particles in the foam skeleton generated higher thermal conductivity values. This was expected since thermal conductivity is strongly influenced by the characteristic length path for heat transfer in the composite, mainly determined by the average inclusion size (see Equation 5). ´The presence of a TiC interlayer between diamond and Mg, whose thickness was as narrow as possible, was clearly necessary to overcome the thermal conductivity of the reference material (a Mg foam). The explanation is that any thermal inclusion in a matrix has to accomplish $K_r^{eff} > K_m$, achieved for a certain minimum particle radius [35]. By taking the values of 1.41×10^6 W/m^{2}K and 8.43×10^7 W/m^{2}K for h, which corresponded to the Mg-diamond and Mg-TiC-diamond interfaces, respectively, and by using the data in Table 1 and Equation 5, the critical value for the diamond particle diameter was calculated as

248 μm for the uncoated diamond particles and as 4.2 μm for the TiC-coated diamond particles. Since the two types of MBD4 diamond particles used herein had diameters of 36 μm and 24 μm (Table 3), only those materials that contained TiC-coated diamond particles were expected to show a thermal conductivity higher than Mg. Although this is true, it is important to realize that TiC is a low thermal conductivity phase. Hence calculations yielded the best results for the foams that contained the diamond particles coated with the thinnest TiC coating considered herein (50 nm). The highest value of thermal conductivity consequently corresponded to a foam that contained MBD4 400-500 diamond particles in the 30 vol% proportion coated with a continuous 50 nm layer of TiC. This is in line with the findings of Table 5, where the experimental thermal conductivity values for the manufactured materials are presented. For better comparisons, the calculated and experimental values are plotted in Figure 8b. In general, an almost perfect agreement was reached between both sets of values. It seemed, however, that the experimental values displayed a slight systematic tendency (within error) to be lower than those calculated. Although the explanation for this phenomenology is not simple, it could be related to the fact that metal did not completely cover the diamond particles located at the surface of the pores (see Figure 7e). This could mean that some of these particles behaved as inefficient thermal inclusions given a diminished metal-particle interface. Therefore, the material exhibited poorer overall thermal conductivity.

4.5 Thermal performance of magnesium-diamond composite foams in heat dissipation by air-forced convection

Heat dissipation performance on active convective cooling was characterised for some of the foam materials manufactured in this paper. Figure 9 shows the results for a foam

sample that contained 30 vol.% MBD4 400-500 diamond particles with a TiC coating of 50 nm (sample with a thermal conductivity of 82 W/mK). The temperatures of both the material and air are seen in Figure 9a for two different air flows (3 l/min and 20 l/min). The higher the air flow imposed, the lower the temperature of the material and that of the air evacuated from the material at any distance from the heat source.

The heat dissipation power densities for different air flows are shown in Figure 9b. This figure also includes the measurements taken on the aluminium and Mg foams with the same pore characteristics for comparison reasons. The presence of TiC-coated diamond particles was clearly favourable as it allowed heat dissipation power densities above 13 W/cm^2 for 20 l/min. This power dissipation was much higher than those obtained with the equivalent magnesium or aluminium foams, for which maximum heat dissipation power densities of 8.5 W/cm^2 and 11 W/cm^2, respectively, were measured for 20 l/min. The data available in bibliography on power densities of dissipated heat for open-cell foams are very scarce and their comparison must be made only for equivalent samples because the thermal performance of a given foam material depends on several parameters; e.g., density, pore size distribution, cell connectivity, tortuosity, strut size, density and geometry, surface roughness, etc. [36].

Further improvements to the heat dissipation performance of these materials could be made by working with coating technologies that allow thinner TiC coatings to be obtained and by optimising the manufacture conditions, which may play a key role in the formation of better thermal interfaces: temperature, contact time, applied pressure and solidification rate.

Conclusions

Novel Mg-diamond composite foams have been successfully produced by the replication method by infiltrating liquid Mg into preforms made up of large (360 μm) NaCl particles that touch one another and small (either 24 or 46 mm) diamond particles located in the voids left by NaCl particles. Since the presence of diamond is not a sufficient condition to increase the thermal conductivity of Mg, due to small particle dimensions, it was necessary to generate a multicomponent Mg-TiC-diamond interface by coating diamond particles with a 50 nm TiC layer. The manufactured composite foam materials obtained high thermal conductivity values (up to 82 W/mK) and achieved good thermal performance for active convective cooling, which was almost two times higher than their equivalent magnesium foams and twenty per cent superior to that of conventional aluminium foams (values obtained for the samples that contained the 30 vol.% TiC-coated MBD4 400-500 diamond particles). Such outstanding properties make these novel materials appealing for the most current demanding heat sink applications and open pathways to solutions for emerging challenges in active thermal management.

Acknowledgement

The author acknowledges financial support from "Ministerio de Economía y Competitividad" trough project MAT2016-77742-C2-2-P).

References

[1] Schelling, P.K., Shi, L., Goodson, K.E., 2005. Managing heat for electronics. Materials Today. June, 30–35.

[2] Zweben, B.C., Materials, A.T., 2006. Thermal materials solve power electronics challenges. Power Electron. Technol. February, 40–47.

[3] Mallik, S., Ekere, N., Best, C., Bhatti, R., 2011. Investigation of thermal management materials for automotive electronic control units. Appl. Therm. Eng. 31, 355–362.

[4] Monje, I.E., Louis, E., Molina, J.M., 2013. Optimizing thermal conductivity in gas-pressure infiltrated aluminum/diamond composites by precise processing control. Compos. Part A Appl. Sci. Manuf. 48, 9–14.

[5] Molina-Jordá, J.M., 2015. Design of composites for thermal management: Aluminum reinforced with diamond-containing bimodal particle mixtures. Compos. Part A Appl. Sci. Manuf. 70, 45–51.

[6] Monje, I.E., Louis, E., Molina, J.M., 2016. Interfacial nano-engineering in Al/diamond composites for thermal management by in situ diamond surface gas desorption. Scr. Mater. 115, 159–163.

[7] Molina-Jordá, J.M., 2015. Nano- and micro-/meso-scale engineered magnesium/diamond composites: Novel materials for emerging challenges in thermal management. Acta Mater. 96, 101–110.

[8] Han, X.-H., Wang, Q., Park, Y.-G., T'Joen, C., Sommers, A., Jacobi, A., 2012. A review of metal foam and metal matrix composites for heat exchangers and heat sinks. Heat Transf. Eng. 33, 991–1009.

[9] Shih, W.H., Chiu, W.C., Hsieh, W.H., 2006. Height effect on heat-transfer characteristics of aluminum-foam heat sinks. J. Heat Transfer 128, 530–537.

[10] Mancin, S., Zilio, C., Cavallini, A., Rossetto, L., 2010. Heat transfer during air flow in aluminum foams. Int. J. Heat Mass Transf. 53, 4976–4984.

[11] Zaragoza, G., Goodall, R., 2013. Metal foams with graded pore size for heat transfer applications. Adv. Eng. Mater. 15, 123–128.

[12] Zhao, C., Hodson, H., Kim, T., Lu, T., 2004. Thermal transport in high porosity cellular metal foams. J. Thermophys. Heat Transf. 18, 309–317.

[13] Mancin, S., Zilio, C., Diani, A., Rossetto, L., 2012. Experimental air heat transfer and pressure drop through copper foams. Exp. Therm. Fluid Sci. 36, 224–232.

[14] Gallego, N.C., Klett, J.W., 2003. Carbon foams for thermal management. Carbon N. Y. 41, 1461–1466.

[15] Straatman, A.G., Gallego, N.C., Yu, Q., Betchen, L., Thompson, B.E., 2006. Forced convection heat transfer and hydraulic losses in graphitic foam. J. Heat Transfer 129, 1237–1245.

[16] Haghighi, M., Kasiri, N., 2010. Estimation of effective thermal conductivity enhancement using foam in heat exchangers based on a new analytical model. Brazilian J. Chem. Eng. 27, 127–135.

[17] Yang, W., Peng, K., Zhu, J., Li, D., Zhou, L., 2014. Enhanced thermal conductivity and stability of diamond/aluminum composite by introduction of carbide interface layer. Diam. Relat. Mater. 46, 35–41.

[18] Zhang, Y., Zhang, H.L., Wu, J.H., Wang, X.T., 2011. Enhanced thermal conductivity in copper matrix composites reinforced with titanium-coated diamond particles. Scr. Mater. 65, 1097–1100.

[19] Chung, C.-Y., Chu, C.-H., Lee, M.-T., Lin, C.-M., Lin, S.-J., 2014. Effect of titanium addition on the thermal properties of diamond/Cu-Ti composites fabricated by pressureless liquid-phase sintering technique. ScientificWorldJournal. 2014, 713537.

[20] Ferri, J.M., Molina, J.M., Louis, E., 2015. Fabrication of Mg foams for biomedical applications by means of a replica method based upon spherical carbon particles. Biomed. Phys. Eng. Express 1, 045002.

[21] Yu, A.B., Zou, R.P., 1998. Prediction of the porosity of particle mixtures. KONA Powder Part. J. V, 68–81.

[22] Molina, J.M., Saravanan, R.A., Arpón, R., García-Cordovilla, C., Louis, E., 2002. Pressure infiltration of liquid aluminium into packed SiC particulate with a bimodal size distribution. Acta Mater. 50, 247–257.

[23] Finkers, H.J., Hoffmann, A.C., 1998. Structural ratio for predicting the voidage of binary particle mixtures. AIChE J. 44, 495–498.

[24] Gale, W.F., Totemeier, T.C. (Eds.), Smithells Metals Reference Book, eight ed., Elsevier, 2004.

[25] Shackelford, J.F., Alexandre, W., Materials Science and Engineering Handbook, third ed., CRC Press, 2001.

[26] Molina, J.M., Narciso, J., Weber, L., Mortensen, A., Louis, E., 2008. Thermal conductivity of Al–SiC composites with monomodal and bimodal particle size distribution. Mater. Sci. Eng. A 480, 483–488.

[27] Tavangar, R., Molina, J.M., Weber, L., 2007. Assessing predictive schemes for thermal conductivity against diamond-reinforced silver matrix composites at intermediate phase contrast. Scr. Mater. 56, 357–360.

[28] Breval, E., Cheng, J., Agrawal, D.K., 2000. Development of titanium coatings on particulate diamond . J. Am. Ceram. Soc. 108, 2106–2108.

[29] Molina, J.M., Prieto, R., Narciso, J., Louis, E., 2011. Dispositivo y procedimiento de utilización del mismo para la infiltración de preformas porosas con metals líquidos de alta presión de vapour, Spanish Application Patent ES 2410904 A1.

[30] Molina, J.M., Prieto, R. Narciso, J., Louis, E., 2011. Device and method for using same to infiltrate porous preforms with liquid metals having high vapour pressure, International Application Patent WIPO 2013/093129 A1.

[31] Molina, J.M., Piñero, E. Narciso, J., García-Cordovilla, C., Louis, E., 2005. Liquid metal infiltration into ceramic particle preforms with bimodal size distributions, Curr. Opin. Solid State Mater. Sci. 9, 202–210.

[32] Lee, J.-H., Lackey, W.J., Benzel, J.F., 1996. Ternary packing of SiC and diamond particles in ethanol. J. Mater. Res. 11, 2804–2810.

[33] Lipatnikov V.N., Gusev A.I., 1999. Dependence of the resistivity of nonstoichiometric titanium carbide TiC y on the density and distribution of carbon vacancies. J. Exp. Theor. Phys. 70, 294–300.

[34] Feldhoff, A., Pippel, E., Woltersdorf, J., 1999. Carbon-fibre reinforced magnesium alloys : nanostructure and chemistry of interlayers and their effect on mechanical. J. Microsc. 196, 185–193.

[35] Davis, L.C., Artz, B.E., 1995. Thermal conductivity of metal-matrix composites. J. Appl. Phys. 77, 4954.

[36] Lefebvre, B.L., Banhart, J., Dunand, D.C., 2008. Porous metals and metallic foams : Current status and recent developments. Adv. Eng. Mater. 775–787.

Figure captions

Figure 1. Scanning electron microscopy images of the NaCl (a) and MBD4 diamond (b) particles; (c) and (d) are magnified images of the TiC-coated diamond particles; (e) and (f) are drawings to illustrate the replication method.

Figure 2. Setup of the characterisation of heat dissipation performance on active convective cooling of foam samples.

Figure 3. Contour curves of the calculated reinforcement volume fraction (V) for the NaCl+diamond bimodal mixtures over the whole range of NaCl particles fraction (X_{NaCl}) as a function of the ratio of particle diameters R (a); (b) is a magnification of figure (a) within the region of interest. Dots denote experimental values.

Figure 4. Contour curves of the calculated values of h (in log scale) as a function of thermal conductivity and thickness of the TiC coating for magnesium-TiC-diamond composites. The previous experimental value encountered in [7] is indicated.

Figure 5. AES elemental depth profile of TiC-coated diamond particles.

Figure 6. X-ray diffraction pattern of the Dc diamond particles (MBD4 400/500) coated with TiC.

Figure 7. Images of magnesium-diamond composite foams: (a) and (b) are photographs of cylindrical samples; (c-h) are SEM micrographs of the magnesium-diamond composite foams that contain as-received diamond particles and show different features: foam structure before (c) and after (d) NaCl dissolution, diamond particles in the struts of the foam (e and f), close-up detail of the magnesium-diamond interface that reveals precipitates on the diamond surface (g), and EDX elemental mapping of the image in g (h); and (i-j) are close looks at the TiC-coated diamond particle surfaces located in the struts of the foam – in (j) fine precipitates similar to those observed in (h) are also found. Samples were prepared by fracture (c-f) or fracture followed by metal electroetching (g-j).

Figure 8. (a) A graph of the calculated thermal conductivity versus the fraction of diamond particles (X_D) of the magnesium-diamond composite foams for the MBD4 diamond particles with R=10 and R=15 and for various TiC coating thicknesses; (b) a graph of experimental thermal conductivity versus the values calculated for the magnesium-diamond composite foams manufactured in the present work – for comparison reasons, the value of an equivalent Mg foam is also indicated.

Figure 9. Graphs showing heat dissipation performance on active convective cooling of the magnesium-diamond composite foam that contained 30 vol.% MBD4 400/500 diamond particles with a TiC coating of 50 nm: (a) is a graph of the temperatures of the foam (solid) and outcoming air (air) vs. the adimensional height of the sample (z/H, where H=15 mm) for different air flow rates; (b) is a graph of the heat power density dissipated vs. air flow rate – the behaviour of the porous-equivalent aluminium and magnesium foams is also indicated for comparison reasons (aluminium foams were processed by the same replication method at an infiltration temperature of 740ºC).

Tables

Table 1. Thermal conductivity K and interface thermal conductance h for different phases and interfaces.

		K (W/mK)	h (W/m^{2}K)
Phases	Mg (99.99%)	156 [27]	-
	Diamond$_{MBD4}$	1450 [5,7]	-
	TiC	17-31[28]	-
Interfaces	Mg-Diamond$_{MDB4}$	-	1.41×10^6 [7]
	Mg-TiC	-	1.34×10^8 [7]
	TiC-Diamond$_{MBD4}$	-	6.18×10^8 [7]

Table 2. Nominal major impurities of the magnesium metal (>99.9 wt%).

	Fe	Mn	Al	Si
concentration (ppm)	<280	<170	<70	<50

Table 3. Main characteristics of NaCl and diamond particles: D (in μm) is the average diameter, AR is the aspect ratio, defined as the ratio between the longest and shortest diameter in the same object; V is the packing volume fraction (with an associated error of ±0,01) and R is the ratio of particle diameter in relation to the diameter of the coarsest (NaCl) particles.

Code	Particle type	D	AR	V	R
S	NaCl	362	1.4	0.60	1
Dc	MBD4 400/500	36	1.1	0.61	10
Ds	MBD4 600/700	24	1.2	0.61	15

Table 4. Composition of salt mixture for the TiC coatings.

	Ti	KCl	NaCl	$CaCl_2$
composition (wt%)	4.0	50.9	41.3	3.8

Table 5. Properties of manufactured materials. V [-] is the packing volume fraction. δ_c (g/cm^3) and S (%) are the density and metal saturation in the materials prior to NaCl dissolution. δ_f (g/cm^3) is the density of foams (after NaCl dissolution) and K their thermal conductivity (W/mK). Associated errors are 2% for δ_i and 5% for K. The error in S is indicated for each case.

X_D	Preform	V	δ_c	S	δ_f	K
0	S	0.60	2.00	98±2	0.70	37
0.1	S+Ds	0.66	2.09	96±4	0.81	29
	S+Dc	0.66	2.10	97±3	0.82	28
	S+TiC-Ds	0.64	2.09	97±3	0.86	40
	S+TiC-Dc	0.64	2.08	97±3	0.85	44
0.15	S+Ds	0.69	2.18	98±2	0.90	25
	S+Dc	0.69	2.17	97±3	0.91	32
	S+TiC-Ds	0.70	2.18	97±3	0.89	49
	S+TiC-Dc	0.69	2.17	97±3	0.90	44

0.2	S+Ds	0.70	2.20	95±5	1.02	20
	S+Dc	0.71	2.22	96±4	1.00	23
	S+TiC-Ds	0.74	2.26	98±2	0.99	45
	S+TiC-Dc	0.73	2.25	97±3	0.99	55
0.25	S+Ds	0.74	2.30	96±4	1.11	22
	S+Dc	0.74	2.29	95±5	1.08	23
	S+TiC-Ds	0.75	2.32	98±2	1.10	56
	S+TiC-Dc	0.76	2.31	95±5	1.08	62
0.3	S+Ds	0.77	2.40	99±1	1.22	17
	S+Dc	0.77	2.38	97±3	1.22	22
	S+TiC-Ds	0.79	2.39	96±4	1.18	75
	S+TiC-Dc	0.79	2.39	96±4	1.19	82

Figures

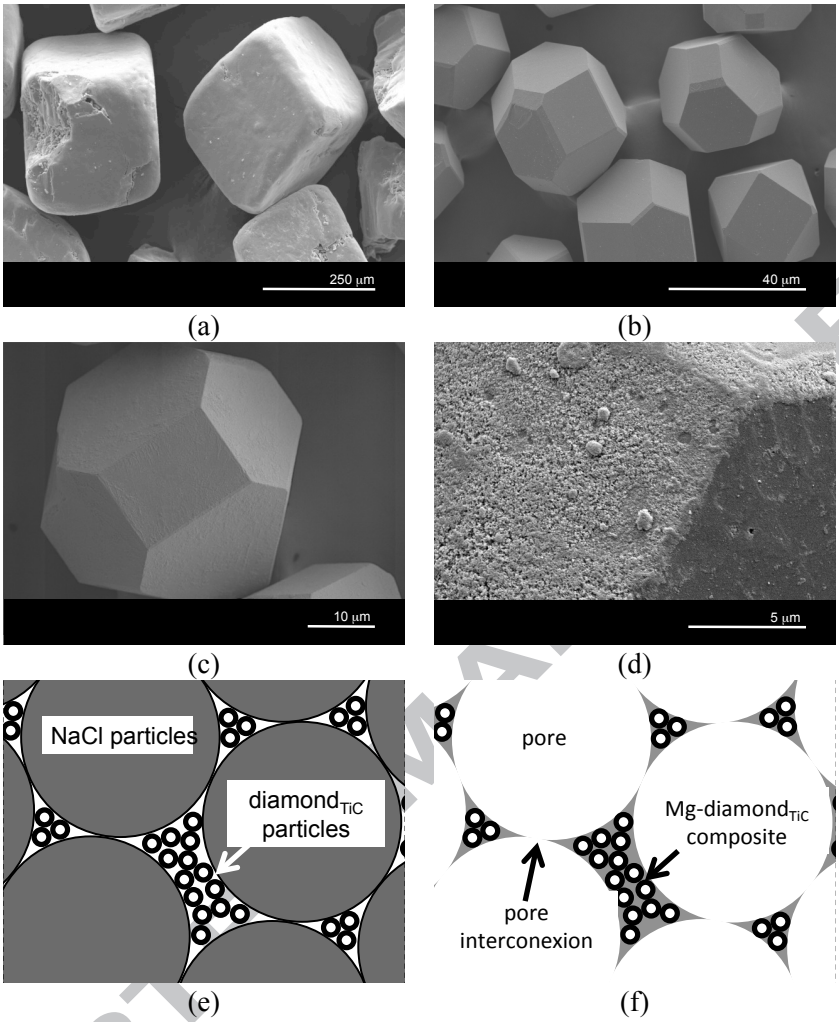

Figure 1

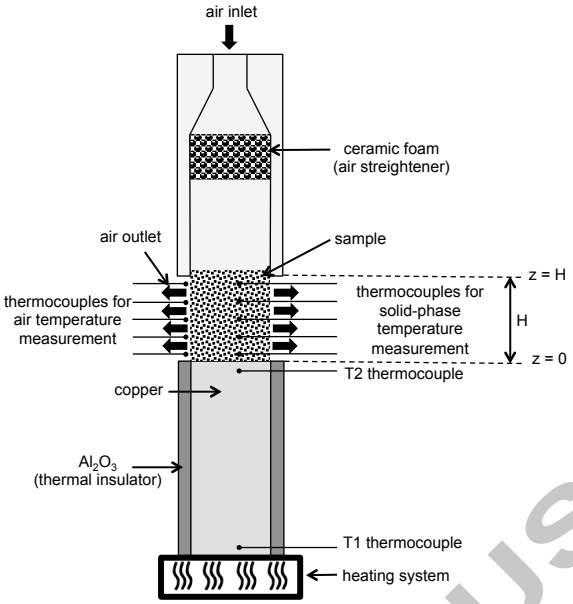

Figure 2

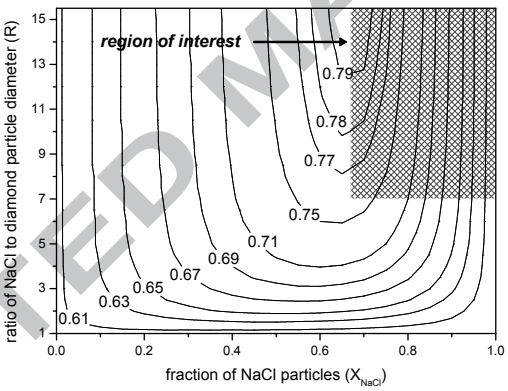

(a)

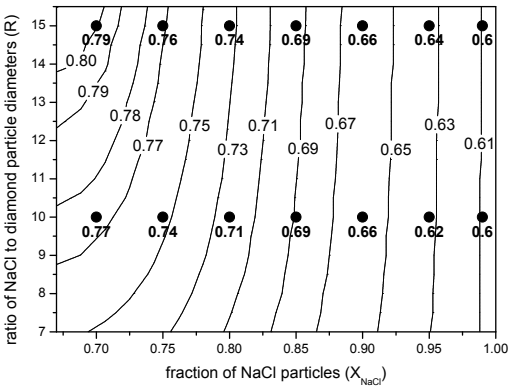

(b)

Figure 3

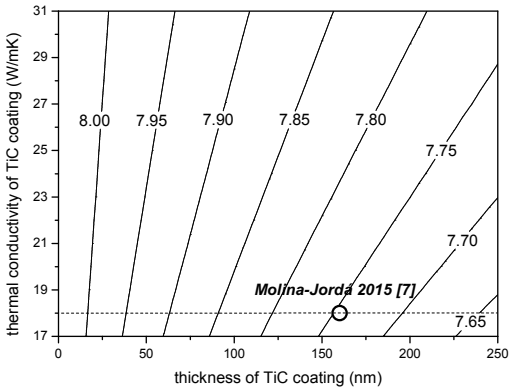

Figure 4

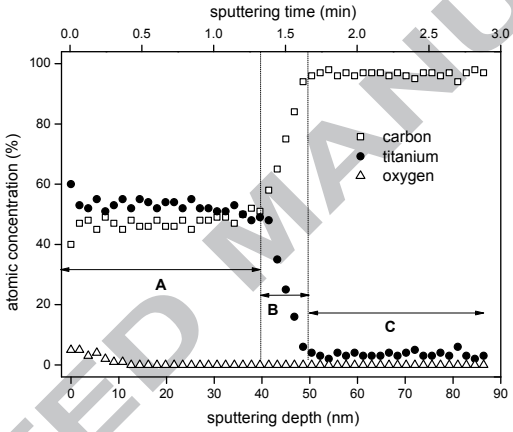

Figure 5

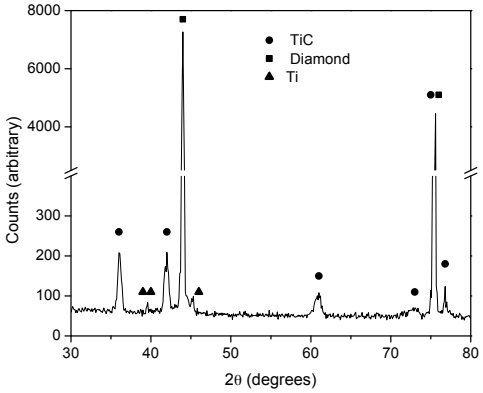

Figure 6

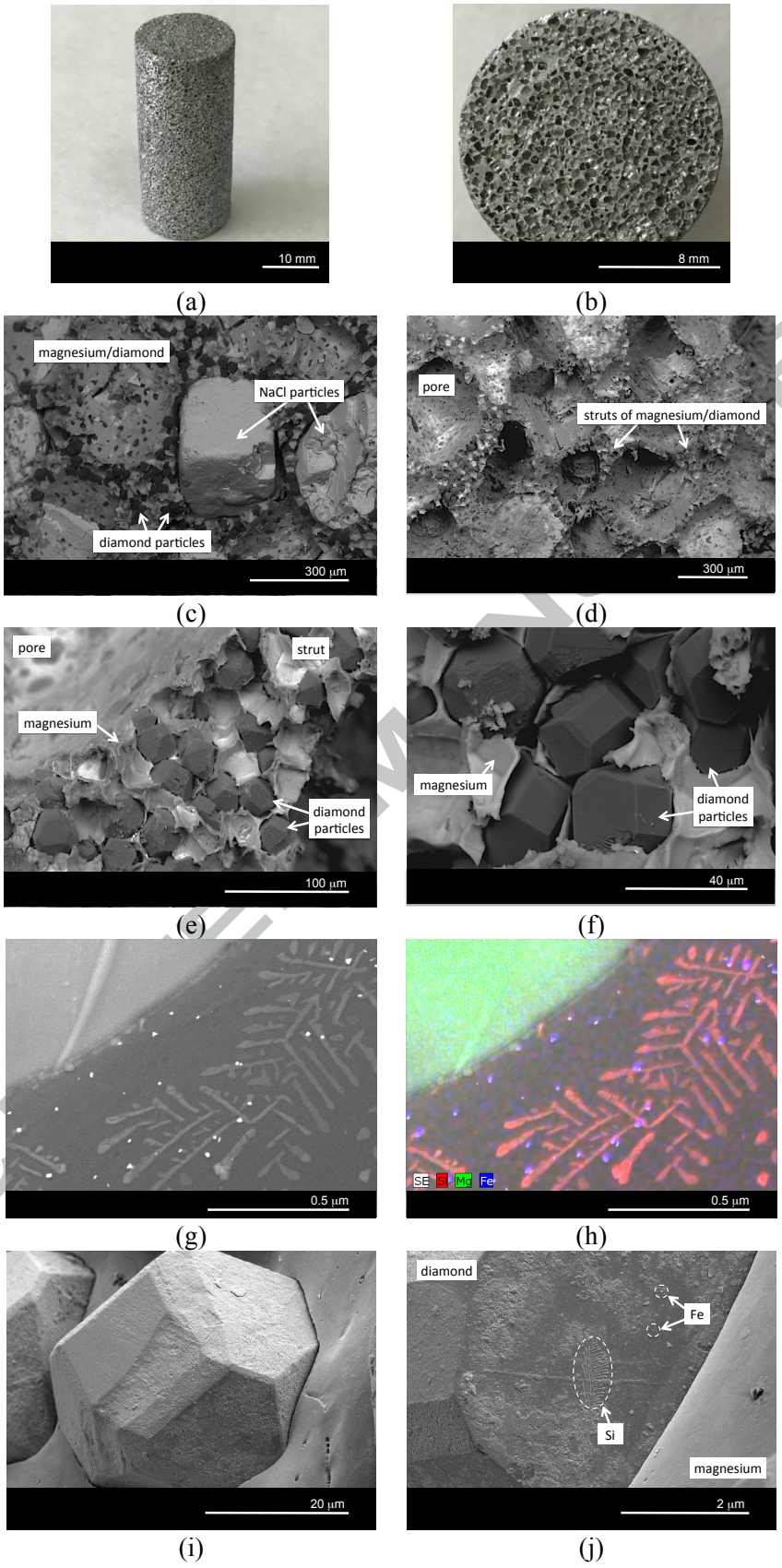

Figure 7

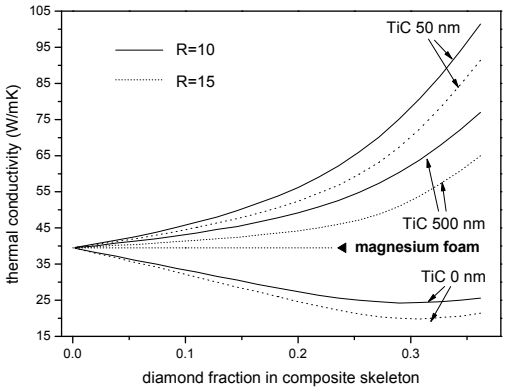

(a)

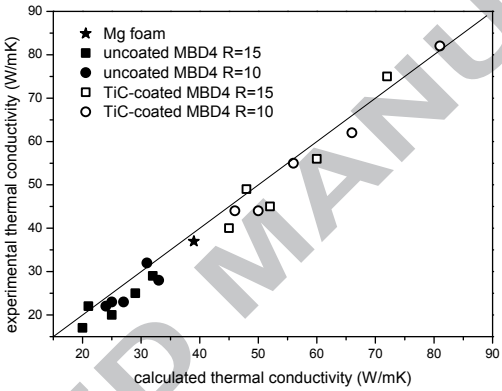

(b)

Figure 8

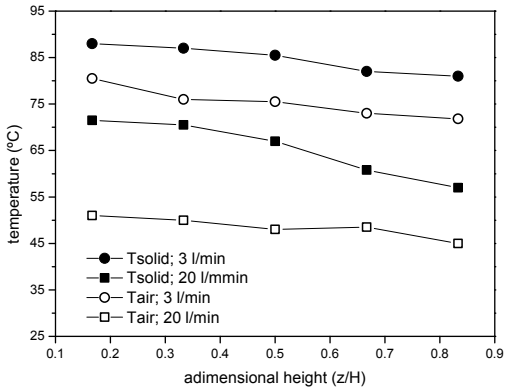

(a)

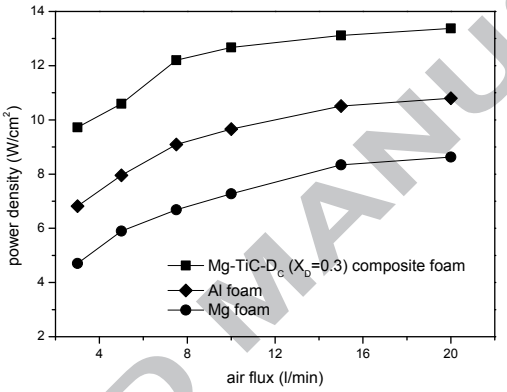

(b)

Figure 9